Humid air generator at LNE-CETIAT: modeling activity

E. Georgin [1], J. Ouazzani [2]

[1] LNE-CETIAT, Villeurbanne, France

[2] ARCOFLUID CONSULTING LLC, Orlando, FL

Abstract

The humid air generator developed at LNE-CETIAT has been designed in 2001 and underwent different upgrade in order to reduce uncertainties. This paper reports the development at the LNE-CETIAT of a software tool for modelling evaporation-condensation phenomena and other heat and mass transport associated with the humid air generator. The tool, based around a commercial computational fluid dynamics package, will be used to increase the efficiency of the LNE-CETIAT primary humidity generator and design new generator as well. The numerical simulations have been done with the general finite volume code PHOENICS with customization in order to tackle the evaporation/condensation process.

Basically, the first step of this numerical work has been to solve the coupled conservation equations for mass, momentum and energy applied to a cylindrical geometry. In addition as the humid air may be considered like a binary mixture between dry air and water vapor, a specie equation is also solved in order to describe the advection-diffusion of water vapor. At last, as the main purpose deals with humidity, fundamental scalar equations of humidity are also computed. The system studied is a water pool inside a cylinder, the main part of heat and mass exchange appear at the interface level between air and water. Thus an original work has been done about the boundary conditions at the interface to account for the evaporation and/or condensation occurring at this interface in terms of mass and energy sinks and/or sources.

Keywords: Evaporation, Humid air generator, Heat and mass transfer, Numerical simulation

1. Introduction

In order to understand the physics of condensation/evaporation processes in humid air generators, a numerical work has been undertaken. This work deals explicitly with understanding the mechanisms of heat and mass transfer between an air volume and a sheet of water in a cylindrical vessel as shown in Fig. 1a. For the purpose of our study, it is not necessary to consider the full water volume but only the water surface as shown in Fig. 1b. This interface is taken to be non deformable in this study. Let us say that this assumption is well justified in view of the low amplitude velocities generated at this particular interface. The mass transfer due to evaporation/condensation is considered occurring only through the water / air (w/a) interface and neglected at the rigid walls. Whereas for the thermal transfer, all boundaries are considered.. Both mass and heat transfer are expressed with *ad hoc* boundary conditions expressed in the next paragraph. The equilibrium in this system is the result of a complex interplay between mass and heat transfer. Mass transfer is essentially governed by water vapor partial pressure gradient which is the leading boundary condition in the water vapor molecules motion described by a specific specie equation. The interfacial heat transfer and the resulting latent heat exchange are directly linked with the water to vapor interfacial phase change. The interfacial water vapor partial pressure is established by the system temperature. The presence of a partial pressure gradient in the vicinity of the interface and of the air bulk leads to evaporation if $p_{H_2O,\mathrm{int}erface} > p_{H_2O,air}$ (condensation will occur in case of the inverse inequality).

These phenomena (evaporation and condensation processes) are simultaneously present, evaporation may be considered as the driving force and condensation considered as a consequence [1].

The first part of this work has been oriented towards the validation of a case dealing with a pure diffusion model. The case consists of a closed vessel without thermal or forced convections, and where a thermal step is imposed at the boundary. The transition and the equilibrium state, reached by the system, are studied and compared to humid air table [12].

For the second part of this work an eccentric circular airflow inlet and a similar outlet have been opened at the top of the cylinder as shown in Fig. 1b. In this second case the vessel being open, mass and heat transfer could also occur through these opening. A thorough parametric study

has been done by varying temperature difference, inlet mass flow rate and humid air concentration.

2. About the model

This work established the basis of the equations which will be used, in further works, in comparison with some experiences.
The geometry considered is presented in Fig. 2 and we may define the following characteristics for the problem under consideration:

- Internal domain: $\Omega = [0;R]\times[0;2\pi]\times[0;Z]$ with $R = 0.035\,\text{m}$ and $Z = 0.07\,\text{m}$
- Boundary domain: $\Gamma = \Gamma_{top} \cup \Gamma_{wall} \cup \Gamma_{in.terface}$
- Surface normal: $\overrightarrow{n_\Gamma}$
- Space variables: $\text{X} = \begin{pmatrix} \text{r} \\ \theta \\ \text{z} \end{pmatrix}$ with $\begin{matrix} r \in [0;R] \\ \theta \in [0;2\pi] \\ z \in [0;Z] \end{matrix}$ in cylindrical coordinates
- Initial conditions:
  $\vec{\text{V}}(\text{X}, \text{t} = 0) = 0$ velocity (m s^{-1})
  $T(X,t=0) = T_{ini}$ temperature (°C)
  $p(X,t=0) = p_{ini}$ pressure (Pa)
  $\rho(X,t=0) = \rho_{ini}$ density (kg m^{-3})
  $q(X,t=0) = q_{ini}(T_{ini})$ mass fraction defines as $q = \dfrac{m_{vapor}}{m_{air} + m_{vapor}}$
  with m_{vapor} the mass of vapor and m_{air} the mass of air

Boundary conditions will be explained before each studied cases.

2.1. Mathematical model

The local forms of the conservation equations solved are the following:

<u>Continuity equation</u>:

$$\frac{\partial \rho}{\partial t} + \nabla.(\rho \mathbf{V}) = \dot{m} \qquad (1)$$

Where $\dot{m}$ have the dimensions of (kg m^{-3} s^{-1}) and corresponds to the net rate of mass entering in phase i (*e.g.* air) from phase j (*e.g.* liquid water); it may be considered as a sink or source due to phase change.

Momentum equations:

$$\rho\frac{\partial \mathbf{V}}{\partial t}+\left[\rho\mathbf{V}\nabla.\mathbf{V}\right]=-\nabla p-\left[\nabla.\underline{\underline{\tau}}\right]+\vec{f}_{ext} \tag{2}$$

Where $\vec{f}_{ext}$ represents external forces such as gravity and

$\underline{\underline{\tau}}=-\left(\mu\left(\nabla\mathbf{V}+\nabla\mathbf{V}^{T}\right)\right)-\frac{2}{3}\nabla\left(\mu\left(\nabla.\mathbf{V}\right)\right)$ the viscous stress tensor

Energy equation:

$$\rho c_p\frac{\partial T}{\partial t}+\left[\rho\mathbf{V}c_p\nabla T\right]=\nabla\left(\lambda\nabla T\right)+\frac{dP}{dt}+S_{latent\,heat} \tag{3}$$

where λ is the thermal conductivity.

Viscous dissipation can be neglected from equation (3) under the assumption of the low Mach number of the flow considered in this work.

Specie equation:

$$\rho\frac{\partial q}{\partial t}+\left[\rho\mathbf{V}\nabla q\right]=\nabla\left(\rho D_M\nabla T\right) \tag{4}$$

where D_M is the Fickian diffusion coefficient, and q is the mass fraction.

2.2. Scalar quantities related to humid air

We list in this paragraph all the laws and values we have used for humid air.

The density of humid air, $\rho_{h.a.}$ (kg m^{-3}), is derived from the assumption that the gas mixture behaves as perfect gas, as expressed in [3]:

$$\rho_{h.a.}=\frac{M_a}{R\cdot T}\left(p_{tot}-e'+\delta\cdot e'\right) \tag{5}$$

Where the molar mass, from [4], are

$M_a=28.96455\times10^{-3}$ kg mol^{-1}

$M_v=18.01528\times10^{-3}$ kg mol^{-1}

$\delta=\frac{M_v}{M_a}$

e' is the water vapor partial pressure, p_{tot} is the total pressure, R is the perfect gas constant and T is the temperature, δ is molar mass ratio between vapor and air.

The Fickian diffusion coefficient D_M $\left(\text{m}^2\ \text{s}^{-1}\right)$ of water vapor in air [2] is:

$$D_M=\left(11.76\times10^{-6}\cdot T^{1.75}\right)\times10^{-4} \tag{6}$$

The thermal conductivity of humid air $\lambda_{h.a.}$ $\left(\mathrm{W\,m^{-1}\,K^{-1}}\right)$[6] is:

$$\lambda_{h.a.} = 0.02397 + 7.590\times10^{-5}\cdot t \tag{7}$$

The dynamic viscosity of humid air $\mu_{h.a.}$ $\left(\mathrm{Pa\,s}\right)$ is:

$$\mu_{h.a.} = \left(17.19 + 0.0429\cdot t\right)\times10^{-6} \tag{8}$$

The calorific capacity

- Dry air, $c_{p,d.a.}$ $\left(\mathrm{J\,kg^{-1}\,K^{-1}}\right)$, in the temperature range $-93.15\,°\mathrm{C} \le t \le +176.85\,°\mathrm{C}$ and $p_{tot} \approx 10^5$ Pa, from [8], is:

$$c_{p,d.a.} = 1000\cdot 4.1855\cdot\begin{pmatrix} 0.240153004 - 3.5655\times10^{-6}\cdot t \\ +3.088866\times10^{-7}\cdot t^2 - 1.33558\times10^{-9}\cdot t^3 \\ -6.10368\times10^{-12}\cdot t^4 + 3.68759\times10^{-14}\cdot t^5 \end{pmatrix} \tag{9}$$

- Water vapor, $c_{p,H2O\,vap}$ $\left(\mathrm{J\,kg^{-1}\,K^{-1}}\right)$, in the temperature range $-15\,°C \le t \le +100\,°C$ [8] is

$$c_{p,H2O\,vap} = 1000\cdot\begin{pmatrix} 1.888235 + 5.833111\times10^{-4}\cdot t + 1.764098\times10^{-5}\cdot t^2 \\ -1.680476\times10^{-7}\cdot t^3 + 1.22539\times10^{-9}\cdot t^4 \end{pmatrix} \tag{10}$$

- The mixing law of dry air and vapor pressure, $c_{p,a.h}$ $\left(\mathrm{J\,kg^{-1}\,K^{-1}}\right)$ [6] is:

$$c_{p,a.h} = c_{p,d.a.} + q\cdot\left(c_{p,H2O\,vap} - c_{p,d.a.}\right) \tag{11}$$

The latent heat l_v $\left(\mathrm{J\,K^{-1}}\right)$ [10] is:

$$l_v = 2500.002 - 2.273\cdot t - 1.641\cdot t^2 + 5.055\times10^{-6}\cdot t^3 - 4.94\times10^{-8}\cdot t^4 \tag{12}$$

2.3. Features

In this work we make the assumption that the temperature in liquid volume of water is completely homogeneous and does not have temperature gradient in its bulk. This hypothesis is justified due to the low rate of evaporation in this kind of set up.

In each case, the grid spacing has been chosen in order to refine the mesh in the area where the strongest gradients of mass and/or temperature may occur, *i.e.* near the wall and near the interface. The CFD software, PHOENICS, has been used recently in similar topics [11] about the condensation of the water vapor present in the atmosphere.

3. Cases studies

3.1. Closed system

In this case the system starts initially at equilibrium (humid air being fully saturated), and then it underwent a thermal disturbance until the system reaches a second fully saturated state. The thermal disturbance is applied on the top and lateral walls of the domain such as:

$$\begin{cases} T\left(\Gamma_{top} \cup \Gamma_{wall}, t < 5\,s\right) = T_{ini} \\ T\left(\Gamma_{top} \cup \Gamma_{wall}, 5\,s \le t \le 50\,s\right) = T_{ini} + A \cdot t \\ T\left(\Gamma_{top} \cup \Gamma_{wall}, t > 50\,s\right) = T_{final} \end{cases}$$

In the above boundary conditions, the coefficient A represents the amplitude of the slope of the heating ramp and t the time in s.

This disturbance has been chosen in order to represent the temperature change which may be applied by a thermostatic bath. The details of the geometry studied are those presented in Fig. 2 with the inlet and outlet fully replaced by walls. That is to say that the system is fully closed and exchange only thermal energy through Γ_{top}, Γ_{wall} and $\Gamma_{interface}$ and mass through $\Gamma_{interface}$.

The other boundary conditions may be written such as:

$$\begin{cases} \vec{V}\left(X \in \Gamma_{top} \cup \Gamma_{wall} \cup \Gamma_{interface}, t\right) = 0 \\ -\rho \dfrac{D_M}{1-q} \dfrac{\partial q}{\partial \vec{n}}\bigg|_{\Gamma_{interface} t} = m \\ S_{latent\ heat}\big|_{\Gamma_{interface} t} = m\, l_v\ dt \end{cases}$$

where m is the mass evaporated or condensed in the system.

The interface is located at $z = 0$ and the top of the vessel at $z = 0{,}07\ \mathrm{m}$.

Initial conditions are summarized in the table 1 and the results for this closed case are presented in Fig. 3 and 4. These graphics show the profile along the cylinder axis, *i.e.* z coordinate, of the temperature T and the mass fraction q. In both cases as expected the temperature increase faster in the vicinity of the wall where the temperature is imposed. The temperature diffuses and is convected in the internal domain Ω where it reaches the opposite face: .i.e. the liquid-humid air interface. Due to evaporation, an exchange of latent heat occurs at the interface, where the heat flux is modified accordingly leading to the slope seen in the temperature profile of figs 3 & 4. The mass fraction starts to increase in the vicinity of the interface directly related to the evaporation process due to the temperature increase at the interface through the source term of water vapor. The water vapor, similarly to the temperature field, diffuses and is convected in the whole domain until equilibrium is reached. In other words, the air temperature near the interface increases, net evaporation occurs which is reflected in a vapor mole fraction gradient developing from the interface and relaxing as equilibrium is reached at the new temperature.

3.2. Open system

The geometry of this case is exactly the same as the closed case above, except that now the system may exchange heat and mass with the outside through the openings in the top of the domain (see Fig. 2).

3.2.1. Thermal and concentration disturbance

In this case the system starts initially at equilibrium, the humid air is fully saturated, and the flow entering is set to different values, in terms of a temperature and mass fraction, than the internal domain. A thermal disturbance is then applied to the wall system. The system is solved under the assumption of steady state. Thus, the conditions are:

For initials values of dependent and independent variables:

$$\vec{V}\left(X \in \Gamma \cup \Omega,\right) = 0$$
$$T\left(X \in \Gamma \cup \Omega, t = 0\right) = T_0$$
$$q_0\left(X \in \Gamma \cup \Omega\right) = q\left(T_0\right)$$
$$\rho_0\left(X \in \Gamma \cup \Omega\right) = \rho\left(T_0, q_0\right)$$

For the inlet:

$$Q_{m,inlet}\left(\Gamma_{inlet}\right) = Q_m$$
$$T\left(\Gamma_{inlet}, t\right) = T_{inlet}$$
$$q_{inlet}\left(X \in \Gamma_{inlet}\right) = q\left(T_{inlet}\right)$$
$$\rho_{inlet}\left(X \in \Gamma_{inlet}\right) = \rho\left(T_{inlet}, q_{inlet}\right)$$

As expressed in the equations just above, the wall and the domain are set to a constant temperature and to a fixed mass fraction. The inlet conditions in terms of flow, temperature and mass fraction are time independent. The case presented here has an inlet flow rate set to $Q_{m,inlet} = 1.67 \times 10^{-5}$ kg s^{-1}, $T_{inlet} = 10\,°\text{C}, q\left(10\,°C\right) = 7.61 \times 10^{-3}$ $T_0 = 20°\text{C}$, $q_0\left(20\,°C\right) = 1.46 \times 10^{-2}$.

Fig. 5 shows the results obtained in such configuration and presented on a slice located in a plane “r-z”. Fig. 5a shows the velocity profile where we can observe that the forced flow through the inlet is convected normal to the interface. The temperature profile seen in Fig. 5b, exhibit the same shape than the velocity contours in the vicinity of the inlet showing that forced convection dominates natural convection. Note also that the entering mass fraction, in Fig. 5c, is lower than the internal one. In Fig 5c, if one follows a control volume from inlet to outlet, we can notice that there is an increase in volume fraction of the vapor, thanks to the inter-diffusion from richer regions to poorer ones.

In table 2 are reported the synthesis results for different temperature levels in terms of flow rate, mass fraction and efficiency. For efficiency, as mentioned in [5] and [9], we propose to define it based on the mass fraction:

$$\eta = \frac{q_{outlet} - q_{inlet}}{q_{th} - q_{inlet}} \tag{13}$$

where q_{th} is the mass fraction we are supposed to get at interface at steady state. The efficiency function defines whether or not the outlet air is fully saturated with vapor at the interface final equilibrium temperature. When having a constant inflow, in the evaporation configuration, the efficiency is a decreasing function of temperature.

3.2.2. Concentration disturbance

For the same open system as above, we consider now that the temperature at wall and inlet is the same initially as the one in the internal domain, and that the inlet mass fraction is still lower than its bulk value.

$$\vec{V}(X \in \Gamma \cup \Omega,) = 0$$
$$T(X \in \Gamma \cup \Omega, t = 0) = T_0$$
$$q_0(X \in \Gamma \cup \Omega) = q(T_0)$$
$$\rho_0(X \in \Gamma \cup \Omega) = \rho(T_0, q_0)$$

Conditions at the inlet are:

$$Q_{m,inlet}(\Gamma_{inlet}) = Q_m$$
$$T(\Gamma_{inlet}, t) = T_0$$
$$q_{inlet}(X \in \Gamma_{inlet}) = q_{inlet}$$
$$\rho_{inlet}(X \in \Gamma_{inlet}) = \rho(T_0, q_{inlet})$$

The case presented here has an inlet flow rate set to $Q_{m,inlet} = 1.67 \times 10^{-5}$ kg s^{-1}, $T_0 = 10$ °C, $q_{inlet} = 5.40 \times 10^{-3}$.

Fig. 6 is an example of the results we may have in such configuration. The results are presented similarly as in Fig. 5. Fig. 6a shows the velocity profile and where the main noticeable difference is seen on the velocity magnitude. This difference is due to density fields which are not the same between the two cases. Indeed, the density is computed thanks to a perfect gas law, thus the density is close to 1.2 kg.m^{-3} in one case and close to 1.24kg.m^{-3} in the other case which lead to higher velocity in the case where the density is lower. Similarly, the temperature

profile reported in Fig. 6b reveals a slight decrease in temperature. Considering the global mass fraction repartition, it appears that the mass fraction is higher in the interface vicinity (Fig. 6c). It creates a concentration gradient which induces the evaporation and thus the latent heat exchange.

In table 3 is reported the results of some tests carried out. As in the previous case the efficiency is calculated and we notice that when imposing a constant inflow, in the evaporation configuration, this efficiency is a decreasing function of the temperature.

4. Conclusion

This work presented the modeling tool which is under development at LNE-CETIAT. The aim followed is to reinforce the understanding of the phenomena at stake in humid air generator. The model presented here is limited at the humid air part in 3D. The coupled conversation equations of momentum, mass, energy and specie are solved. Thermo physical properties varying with temperature are implemented as well as scalar quantity dedicated to humid air. An original treatment of the boundary conditions allowed us to account for the latent heat exchange and the evaporation process in the temperature range between 0°C and 100°C. The cases studied are divided in close and open systems. Thanks to the closed system the pure diffusion model has been established as well as specific humid air quantity. With the open systems the saturator efficiency may be computed and may give confidence in the design of humid air generator.

Further this model will be developed in order to take into account the condensation phenomenon and to implement a more realistic geometry which fit more closely the real humid air generator.

References

1. J.F. Sacadura, Initiation aux transferts thermiques, Tec & Doc, 1982
2. E.L. Cussler, Diffusion mass transfer in fluid systems third edition, Cambridge 2008
3. B. Cretinon, J. Merigoux, La mesure d'humidité dans les gaz, Monographie du Bureau National de Métrologie, 160 pages, 2000
4. CODATA recommended values of the fundamental physical constants: 2002 / P. J. Mohr and B. N. Taylor, Rev. Mod. Phys. 77, 1, 2005
5. B. Blanquart, Etude et realisation d'un nouveau generateur d'air humide – vers la definition d'une reference en temperature de rosee, These du Conservatoire National des Arts et Metiers, 170 pages, 2001
6. V. Carpentier, Etude pour le développement d'un générateur d'air humide, These de l'Université Blaise Pascal, 161 pages, 2005
7. W. Wagner, A. Kruse, Properties of water and steam, Springer, IAPWS, IF97
8. L'Air Liquide - Encyclopédie des Gaz - ELSEVIER – 1976
9. Gonin F., Blanquart B., Improvement of CETIAT humid air generator in low-range, 5th international symposium on humidity and moisture – ISHM, 2006
10. Tables de référence : ATG - Société du Journal des Usines à Gaz - "Aide-mémoire de l'industrie du gaz" - 3ème édition – 1972
11. Clus O. *et al.*, Comparison of various radiation-cooled dew condensers using computational fluid dynamics, Desalination, 249, 707–712, 2009
12. Blanquart B and Cretinon B., Tables de l'air humide, CETIAT, 2005

Table 1 Initial conditions in the internal domain – closed system configuration

Case 1	Case 2
$T(X,t=0)=10\,^{\circ}\mathrm{C}$	$T(X,t=0)=50\,^{\circ}\mathrm{C}$
$p(X,t=0)=101325$ Pa	$p(X,t=0)=101325$ Pa
$\rho(X,t=0)=1.241$ kg m^{-3}	$\rho(X,t=0)=1.041$ kg m^{-3}
$q(X,t=0)=7.606\times10^{-3}$	$q(X,t=0)=7.995\times10^{-2}$

Table 2 Open system configuration – Thermal and Concentration disturbances

	Case 1 T_0 =20 °C	Case 2 T_0 =30 °C	Case 3 T_0 =40 °C	Case 4 T_0 =50 °C	Case 5 T_0 =60 °C
$Q_{m,inlet}(\Gamma_{inlet})$ (kg s^{-1})	1.67×10^{-5}	1.67×10^{-5}	1.67×10^{-5}	1.67×10^{-5}	1.67×10^{-5}
$q(X \in \Gamma_{inlet})$	7.61×10^{-3}	1.46×10^{-2}	2.66×10^{-2}	4.69×10^{-2}	8.00×10^{-2}
$q(X \in \Gamma_{outlet})$	1.32×10^{-2}	2.42×10^{-2}	4.26×10^{-2}	7.26×10^{-2}	1.20×10^{-1}
$\eta = \frac{q_{outlet} - q_{inlet}}{q_{th} - q_{inlet}}$	8.09×10^{-1}	8.01×10^{-1}	7.90×10^{-1}	7.76×10^{-1}	7.62×10^{-1}

Table 3 Open system configuration – Concentration disturbance

	Case 1 T_0 =20 °C	Case 2 T_0 =30 °C	Case 3 T_0 =40 °C	Case 4 T_0 =50 °C	Case 5 T_0 =60 °C
$Q_{m,inlet}(\Gamma_{inlet})$ (kg s^{-1})	1.67×10^{-5}	1.67×10^{-5}	1.67×10^{-5}	1.67×10^{-5}	1.67×10^{-5}
$q(X \in \Gamma_{inlet})$	5.40×10^{-3}	5.40×10^{-3}	5.40×10^{-3}	5.40×10^{-3}	5.40×10^{-3}
$q(X \in \Gamma_{outlet})$	1.31×10^{-2}	2.30×10^{-2}	3.94×10^{-2}	6.52×10^{-2}	1.05×10^{-1}
$\eta = \frac{q_{outlet} - q_{inlet}}{q_{th} - q_{inlet}}$	8.40×10^{-1}	8.31×10^{-1}	8.19×10^{-1}	8.03×10^{-1}	7.83×10^{-1}

Figure Captions

Fig. 1 Schematic principle of the cylindrical vessel

Fig. 2 Effective geometry modeled

Fig. 3 Closed system (thermal disturbance), mass fraction profiles results for temperature step from 10 °C to 20 °C. Profiles are presented at different time steps

Fig. 4 Closed system (thermal disturbance), mass fraction profiles results for temperature step from 50 °C to 60 °C. Profiles are presented at different time steps

Fig. 5 Open system (thermal and concentration disturbance), velocity, temperature and mass fraction contours for temperature step from 10 °C to 20 °C

Fig. 6 Open system (mass fraction disturbance), velocity, temperature and mass fraction contours

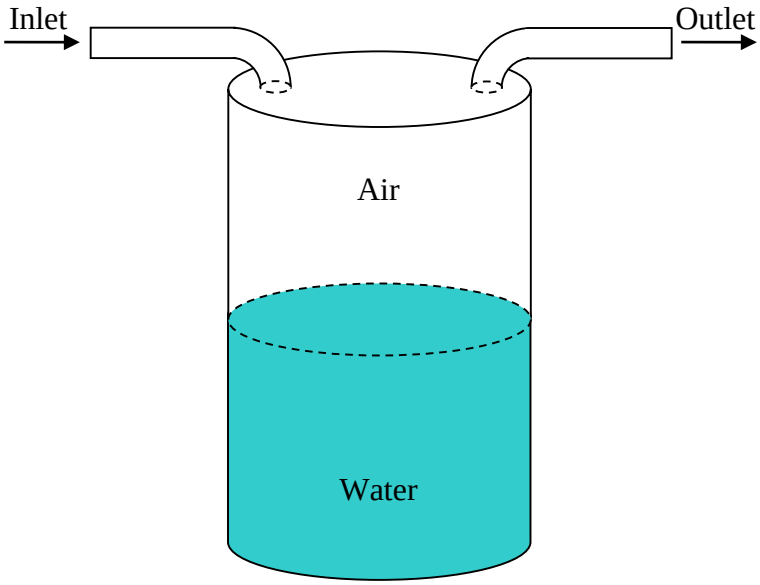

a

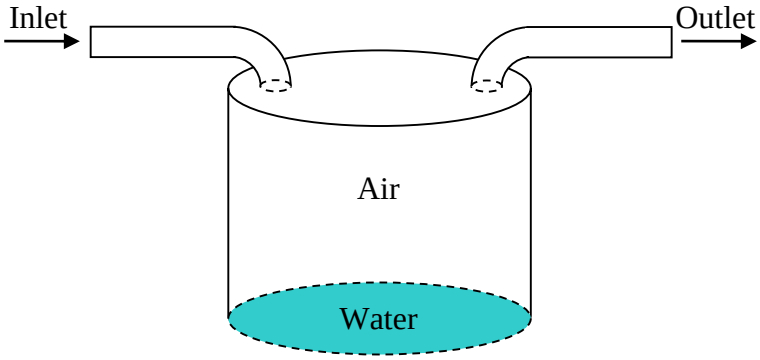

b

Fig. 1.

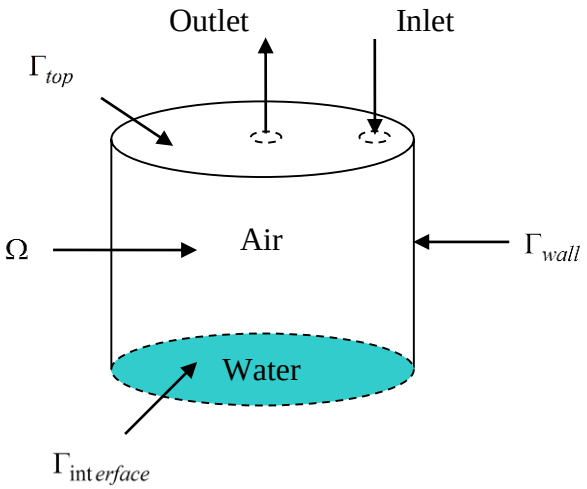
Outlet
Inlet
Γ_{top}
Ω
Air
Γ_{wall}
Water
$\Gamma_{interface}$

Fig. 2.

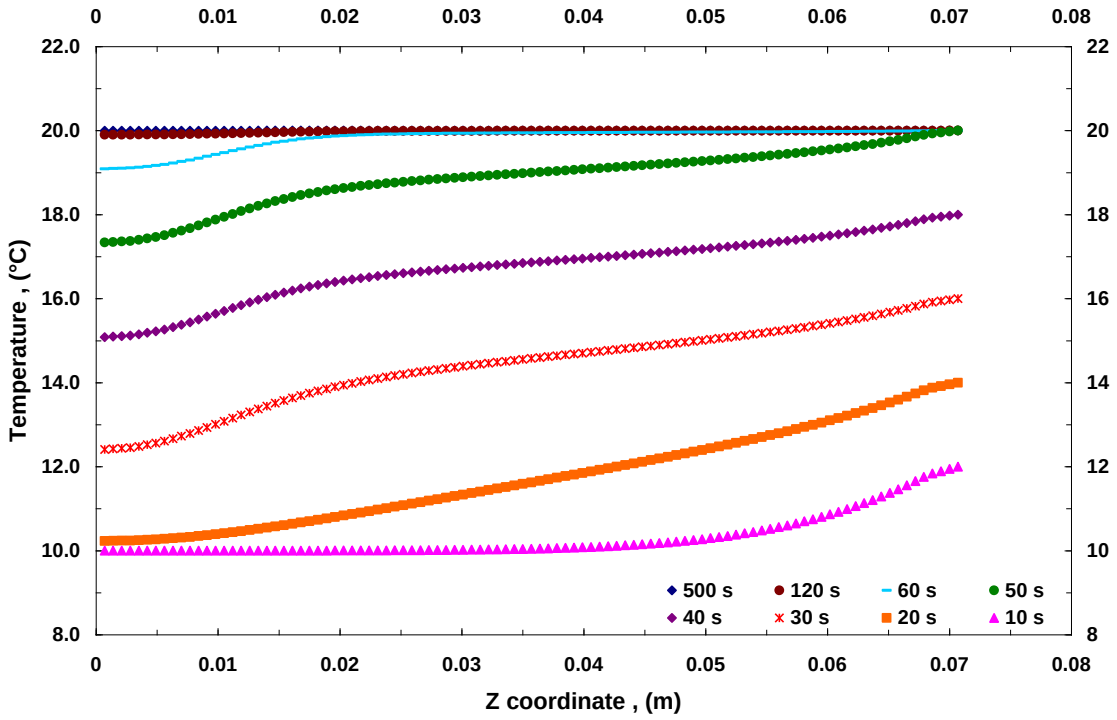
Temperature , (°C)
Z coordinate , (m)
500 s
120 s
60 s
50 s
40 s
30 s
20 s
10 s

a

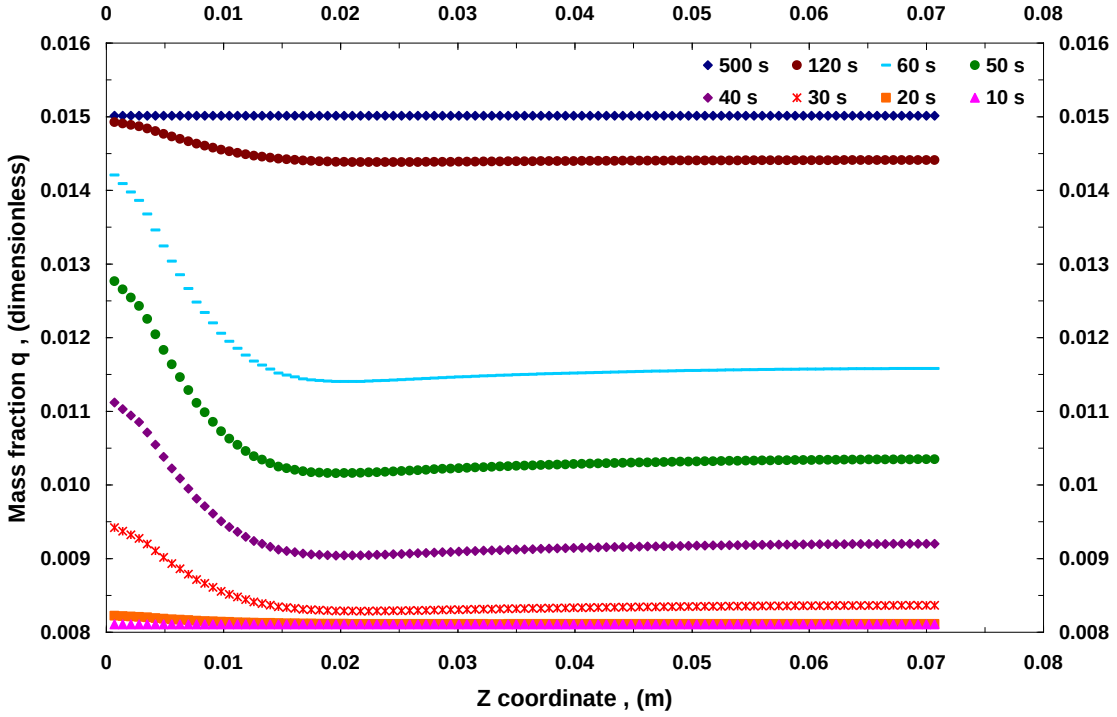
Mass fraction q , (dimensionless)
Z coordinate , (m)
500 s
120 s
60 s
50 s
40 s
30 s
20 s
10 s

b

Fig. 3

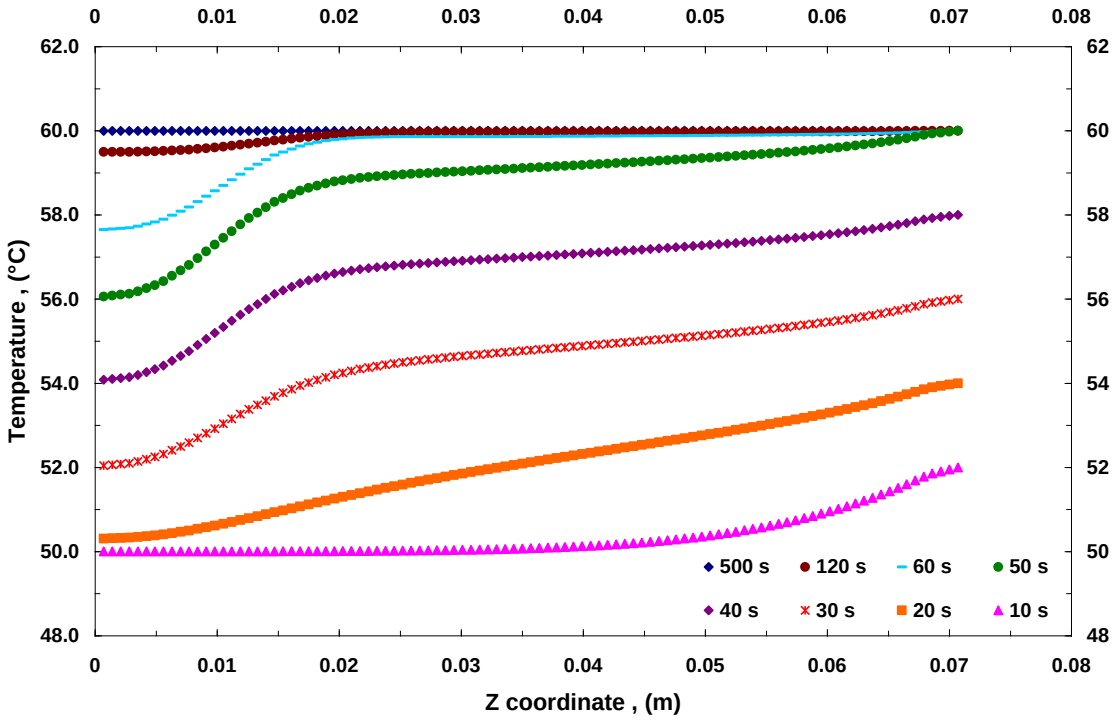
Temperature , (°C)
Z coordinate , (m)
500 s
120 s
60 s
50 s
40 s
30 s
20 s
10 s

a

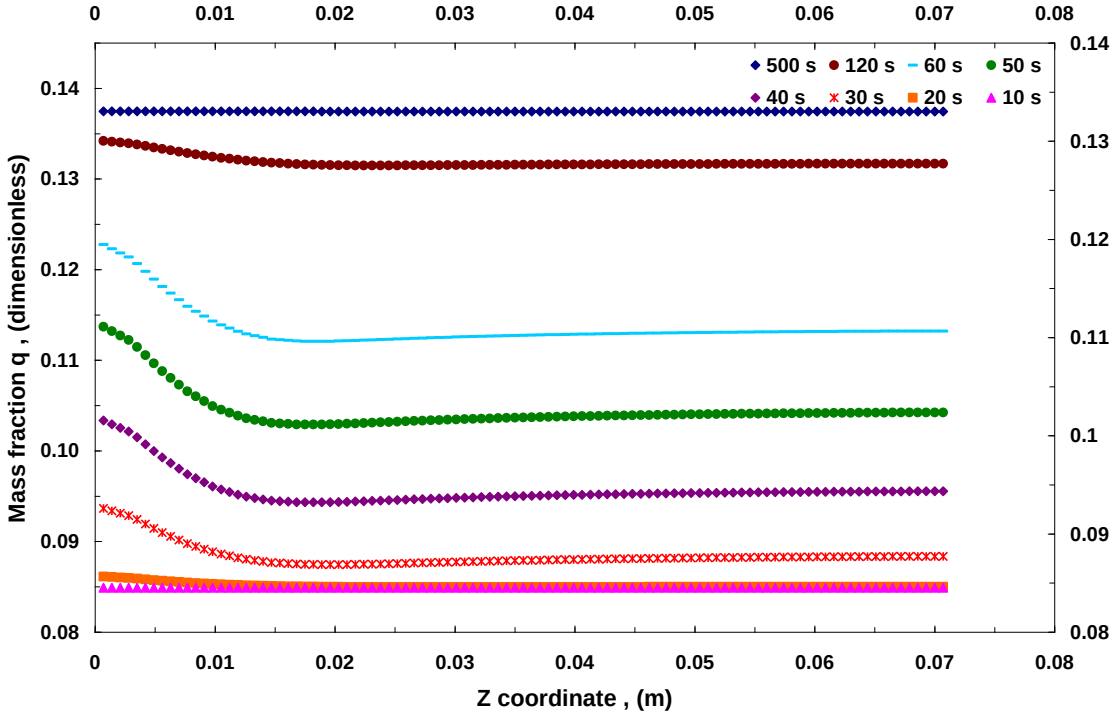
Mass fraction q , (dimensionless)
Z coordinate , (m)
500 s
120 s
60 s
50 s
40 s
30 s
20 s
10 s

b

Fig. 4

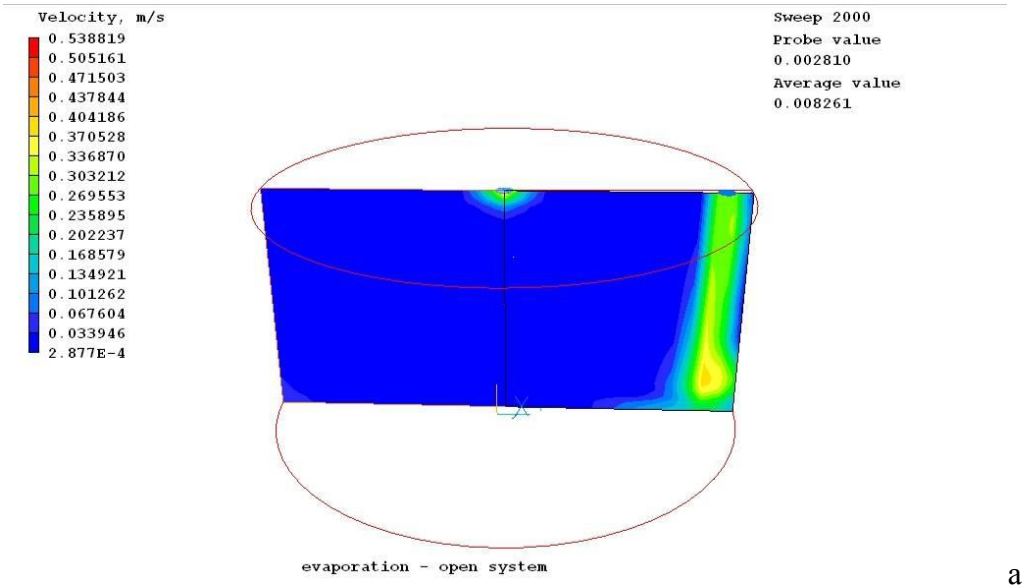
Velocity, m/s
0.538819
0.505161
0.471503
0.437844
0.404186
0.370528
0.336870
0.303212
0.269553
0.235895
0.202237
0.168579
0.134921
0.101262
0.067604
0.033946
2.877E-4
Sweep 2000
Probe value
0.002810
Average value
0.008261
evaporation - open system

a

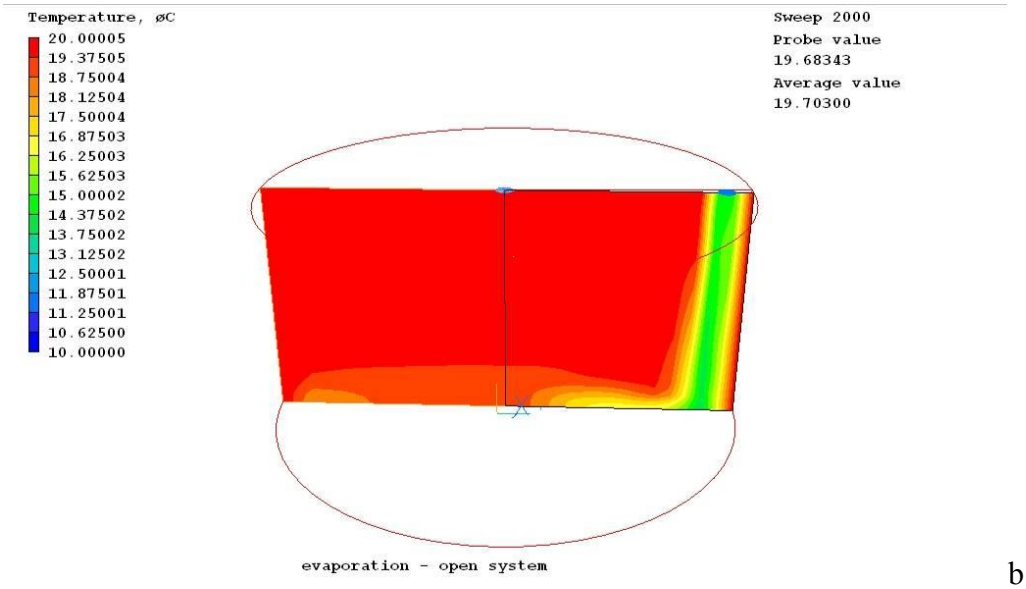
Temperature, øC
20.00005
19.37505
18.75004
18.12504
17.50004
16.87503
16.25003
15.62503
15.00002
14.37502
13.75002
13.12502
12.50001
11.87501
11.25001
10.62500
10.00000
Sweep 2000
Probe value
19.68343
Average value
19.70300
evaporation - open system

b

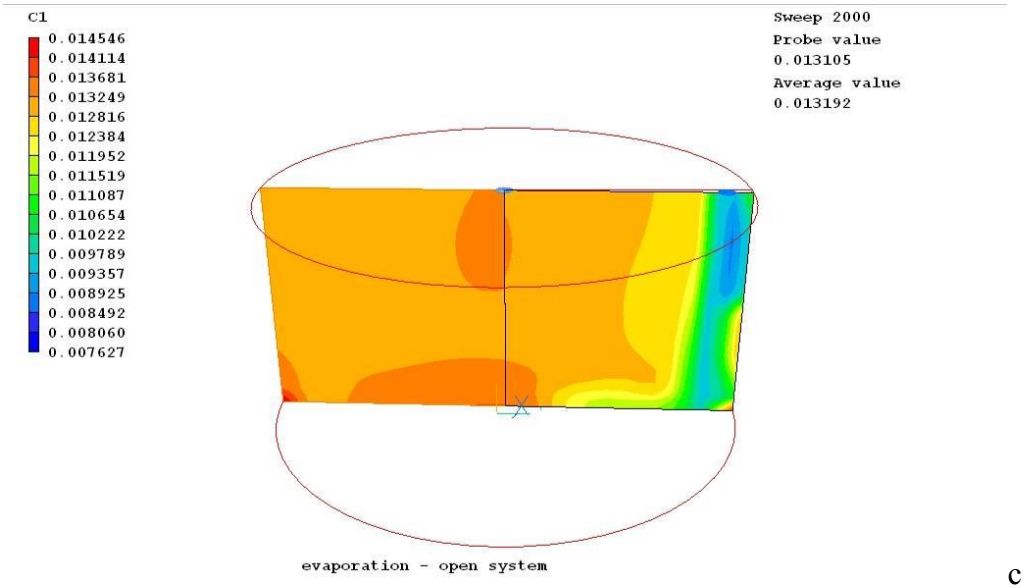
C1
0.014546
0.014114
0.013681
0.013249
0.012816
0.012384
0.011952
0.011519
0.011087
0.010654
0.010222
0.009789
0.009357
0.008925
0.008492
0.008060
0.007627
Sweep 2000
Probe value
0.013105
Average value
0.013192
evaporation - open system

c

Fig. 5.

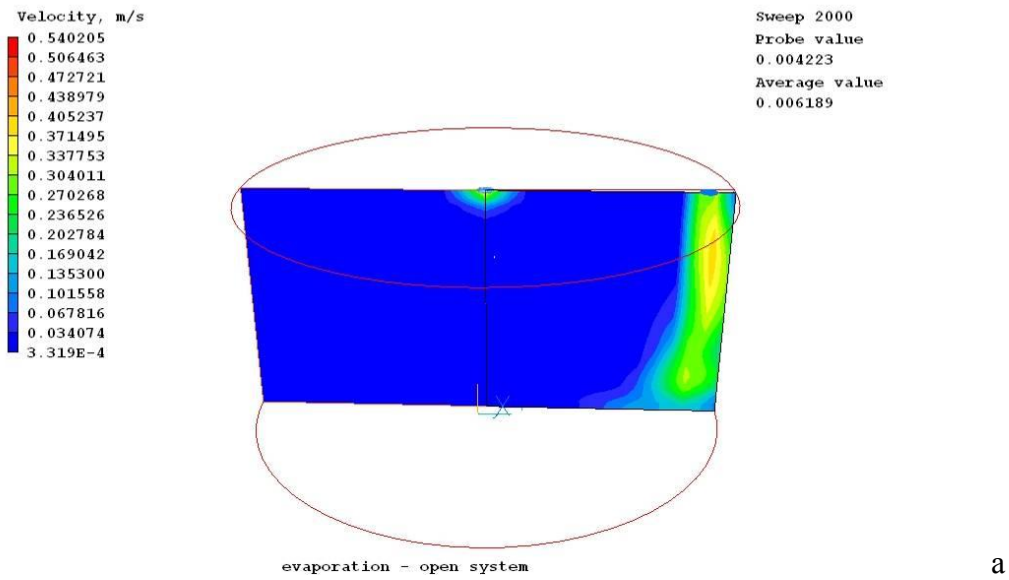
Velocity, m/s
0.540205
0.506463
0.472721
0.438979
0.405237
0.371495
0.337753
0.304011
0.270268
0.236526
0.202784
0.169042
0.135300
0.101558
0.067816
0.034074
3.319E-4
Sweep 2000
Probe value
0.004223
Average value
0.006189
evaporation - open system

a

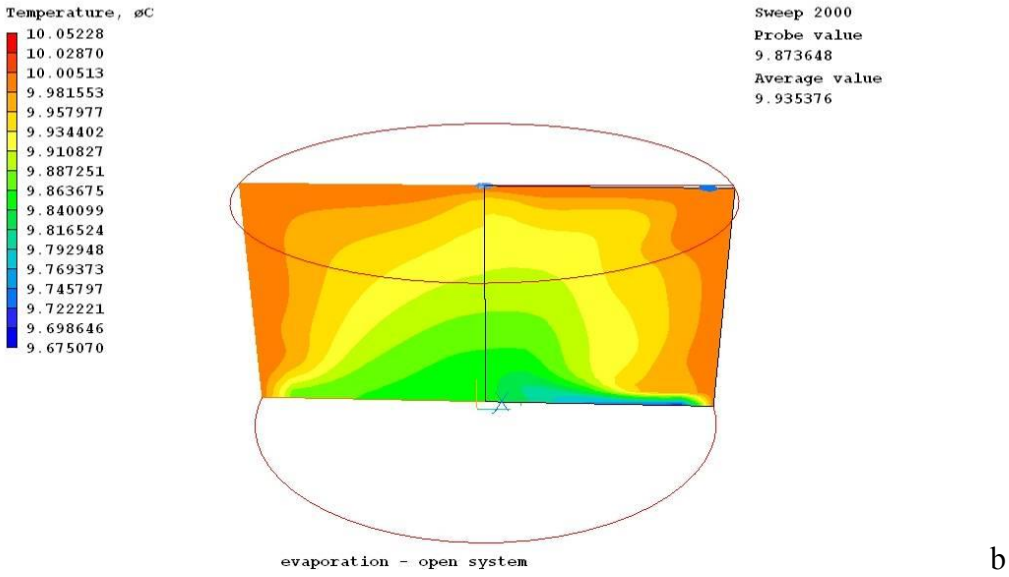
Temperature, øC
10.05228
10.02870
10.00513
9.981553
9.957977
9.934402
9.910827
9.887251
9.863675
9.840099
9.816524
9.792948
9.769373
9.745797
9.722221
9.698646
9.675070
Sweep 2000
Probe value
9.873648
Average value
9.935376
evaporation - open system

b

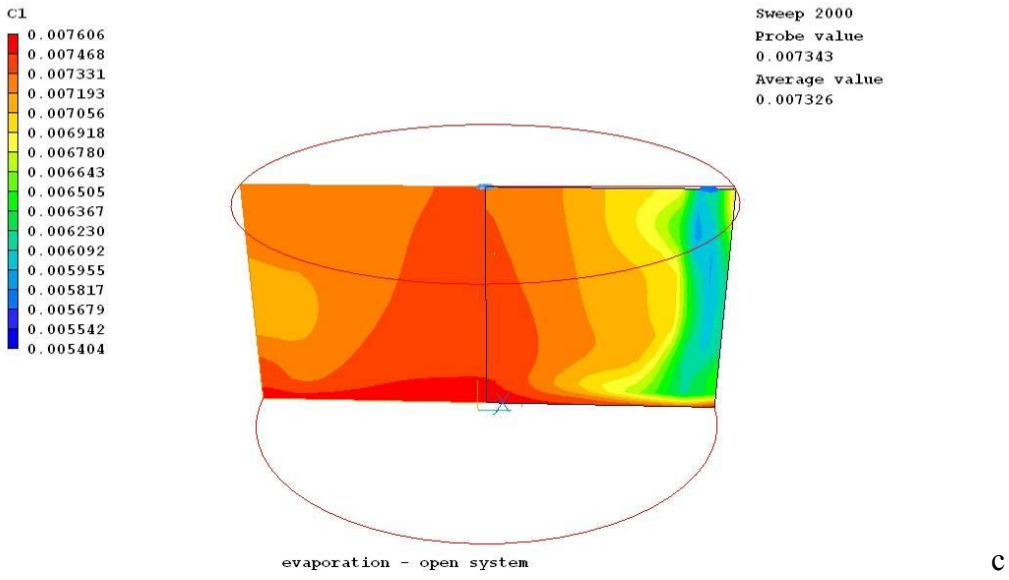
Cl
0.007606
0.007468
0.007331
0.007193
0.007056
0.006918
0.006780
0.006643
0.006505
0.006367
0.006230
0.006092
0.005955
0.005817
0.005679
0.005542
0.005404
Sweep 2000
Probe value
0.007343
Average value
0.007326
evaporation - open system

c

Fig. 6.